



STUDY OF GEOSTROPHIC AND AGEOSTROPHIC COMPONENTS OF CURRENTS THROUGH COMBINED ANALYSIS OF DRIFTING BUOYS AND SATELLITE PRODUCTS



International Chair in Mathematical Physics and Applications

Research Master in Physical Oceanography and Applications

Presented by :

DONFACK Leonel Julio

Faculty of Science and Technology (FAST)

University of Abomey-Calavi (UAC), Cotonou, Republic of Benin

&

University Toulouse III-Paul Sabatier, France

Academic Year 2023-2024

© ICMPA Published in 2024





University of Abomey-Calavi (UAC), BENIN

**Faculty of Science and Technology (FAST)
International Chair in Mathematical Physics and Applications
(ICMPA-UNESCO Chair)**

M. Sc No M. Sc/ICMPA/FAST/UAC/2024.

STUDY OF GEOSTROPHIC AND AGEOSTROPHIC COMPONENTS OF CURRENTS THROUGH COMBINED ANALYSIS OF DRIFTING BUOYS AND SATELLITE PRODUCTS

Research Master in Physical Oceanography and Applications

Presented by :

DONFACK Leonel Julio

Supervisors :

Professor Emmanuel COSME	(IGE/MEOM),
Professor Clément UBELMANN	(GRENOBLE)

Jury :

President :

Examiners :

Rapporteur :

Cotonou, Republic of Benin, September 2024

SPONSORS



Chaire Internationale en
Physique Mathématiques et
Applications

UNIVERSITE
PAUL
SABATIER



TOULOUSE III

Université Paul Sabatier /
Chaires Croisées



Programme Chaires Croisées
(Formation et Recherche en
Océanographie Physique et
Applications en Afrique de
l'Ouest)

DAAD

Deutscher Akademischer Austauschdienst
German Academic Exchange Service

Deutscher Akademischer Austauschdienst
German Academic Exchange Service



Institut des Géosciences de
l'Environnement

STUDY OF GEOSTROPHIC AND AGEOSTROPHIC COMPONENTS OF CURRENTS THROUGH COMBINED ANALYSIS OF DRIFTING BUOYS AND SATELLITE PRODUCTS

Submitted in partial fulfillment of the requirements
for the Master of Science (MSc) degree in Physical Oceanography
at the University Toulouse III & the University of Abomey-Calavi.

Presented by :

DONFACK Leonel Julio

Supervisors :

Professor Emmanuel COSME **(IGE/MEOM),**

Professor Clément UBELMANN **(GRENOBLE)**

Dedication

To my Grandmother

Christine VOTSOP, “MA CHACLEY TEZAR TETE”

.....

To my Mom, the fighter

Philomène SONNA, “MA CHACLEY TEZAR TETE”

.....

To my Father

Thomas FOUAZEU, May God complete in you what He has started.

I hope you are proud to me, Dad

.....

I love you

Remerciements

First of all, I thank the Almighty for the strength He gives me and the mercy He has shown me since my childhood. I can never thank Him enough!

I want to express my heartfelt thanks to Professor Emmanuel Cosme, my internship director, for the trust and support he provided throughout my remote internship due to the cancellation of my stay at IGE (Grenoble) because of administrative difficulties. He was always available for explanations and discussions, sometimes lasting up to four hours. Beyond being an exceptional scientist, he possesses unparalleled humanity. I also appreciate his wise advice and encouragement during tough times. 'Professor Emmanuel is, was, and will remain the mentor I have always wished for in research.' If I were to thank him in detail, I would need several pages, but in short, I sincerely thank him for all he has contributed to me, both scientifically and personally. I also thank Professor Clément Ubelmann, my co-director, for the scientific guidance and the rigorous qualities he instilled in me.

A big thank you to the Institut de Recherche pour le Développement (IRD) and the pioneers of this master's program, without whom this work would not have been possible.

I personally wish to express my sincerest thanks to Professor Norbert HOUNKONNOU, Professor Isabelle DADOU, and Professor BALOITCHA for their fatherly advice and support throughout my academic journey. A special thank you to the mentioned sponsors who make this master's program a comprehensive framework for advancing ocean sciences in Africa.

I would like to thank each jury member who accepted to evaluate this work.

I sincerely thank everyone who dedicated their time to share part of their knowledge with me during this academic year.

I am particularly grateful to all the instructors in this master's program: Gael ALORY, Alexis CHAIGNEAU, Nick Hall, Yves MOREL, Essowe PANASSA, Zacharie SOHOU, Victor OKPEITCHA, Alexei KOURAEV, Pieter VAN-BEEK, Fabrice MESSAL, Marie BONNIN, Adrien COMPTE, Casimir DA ALLADA, Donatus ANGNUURENG, and Frédéric BONOU for enriching us with invaluable knowledge and enabling us to become the ocean scientists we envisioned. I also wish to thank my main supervisors from my

home country, Dr. G. J. AGHOUKENG, Prof. J. MBANG, and Prof. R. D. AYISSI, who, despite their busy schedules, supported me in my program and future career.

I wish to express my deepest obligations to my father, Thomas FOUAZEU, and my mother, Philomène SONNA, who always pray for my success in all aspects of life. Their parental guidance and prayers have shaped the person I hope to become in the near future.

A special mention to the wonders of 'OPA2024', Moussa NDIAYE, my constant partner Héloïse HERON, Célina BENHADDAD (the BOSS of France), DEKPO Atsou, Enock DJORWE, Angèle HOUNKONNOU, and Frédéric AKOTEGNON (the stars of Calavi). A big thank you to the latter two for their warm welcome, which made my stay in Benin truly enjoyable. I also thank the students of the Chair, Jean-Paul ANAGONOU (the student president), Abed-Nego SAMON (the creator of the new CIPMA website), and others for making life in Cotonou easier than expected. I can never thank Willy DIMA and Laeticia Ntangyong enough for their immense support as fellow countrymen in my academic success. I also thank Dr. Nathanael DOSSA, the physical oceanography doctor, for the fruitful discussions and good times shared. Not to forget Ayissi Francis, Roy NGAKALA, former academics, and current doctoral students of CIPMA for their support and availability.

Hats off to my fellow students at the University of Yaoundé I for their support, encouragement, and companionship during my stay: Olivier DONDJIO, Evrard NGUELE, Yvan NDONTSOP, and others. Thank you to my friends Dr. Boris WEMBE, Cédric, and Linda; it is thanks to you that I did not feel homesick for Cameroon.

My deep gratitude goes to my entire family (brothers and sisters, uncles, nieces, nephews, cousins, ...) and especially to my younger sister, Sophie Merveille NGONNANG. I love you all so much; you have given me so much love and responsibility, and I am very happy to be your brother, your guardian angel. I apologize to the whole family for my long absences in the past and in the future during family events.

Finally, I wish to thank everyone who has supported me in one way or another, and whose names I have omitted to mention.

Résumé

L'altimétrie satellitaire fournit une estimation eulérienne à faible résolution des courants géostrophiques, tandis que les bouées dérivantes offrent une mesure lagrangienne des courants de surface, intégrant toutes leurs composantes. Avec l'avènement de nouvelles technologies, telles que les bases de données étendues de drifters et le satellite SWOT, il est pertinent de se demander dans quelle mesure les courants mesurés par les drifters peuvent être corrélés avec ceux observés par les satellites, et si SWOT apporte une amélioration significative par rapport à l'altimétrie classique. Ce travail vise à comparer les données du Global Drifter Program de la NOAA (résolution de $1^\circ \times 1^\circ$) et les produits satellitaires Globcurrent d'AVISO (résolution de $1/4^\circ$) ainsi que SWOT KaRIn et nadir (résolution de $1/60^\circ$), en ajustant les composantes agéostrophiques des courants selon les besoins.

Les oscillations inertielles sont obtenues en filtrant les données des courants des drifters. Nous avons utilisé trois méthodes de filtrage : le filtre linéaire Ubelmann, le filtre médian non linéaire, et le filtre linéaire de Hanning, qui est celui qui donne les résultats les plus cohérents. En effet, les tests montrent que le filtre de Hanning améliore le plus la qualité des courants de surface issus des drifters, avec une amélioration de 14% de la composante géostrophique pour la composante zonale et 16% pour la composante méridionale.

Un filtre glissant spatial puis temporel sur différentes fenêtres est également employé pour filtrer les petites échelles et les hautes fréquences contenues dans SWOT. Les données SWOT sont cohérentes avec les grandes échelles de CMEMS, après un filtrage spatial sur une fenêtre de l'ordre de 1° . La comparaison avec les bouées dérivantes révèle que CMEMS représente très mal les variations des courants des flotteurs. SWOT a une meilleure corrélation pour les courants géostrophiques zonaux, notamment après un lissage temporel de 5 jours, mais n'apporte pas d'amélioration apparente sur la composante méridionale. Ceci est interprété par la dissymétrie de la forme de la trace SWOT, très allongée selon la latitude et de petite largeur selon la longitude. De ce fait, le lissage spatial de 1° est problématique pour la direction zonale et l'estimation des courants méridiens (qui sont obtenus par dérivée zonale). Les simulations ont été faites avec le langage de programmation Python.

Mots clés : Circulation et dynamique océaniques, applications de trajectoire lagrangienne, Bouées dérivantes, Produits satellitaires, Océanographie physique.

Abstract

Satellite altimetry provides a low-resolution Eulerian estimate of geostrophic currents, while drifting buoys offer a Lagrangian measurement of surface currents, incorporating all their components. With the advent of new technologies, such as extensive drifter databases and the SWOT satellite, it is pertinent to question the extent to which drifter-measured currents can be correlated with those observed by satellites, and whether SWOT provides a significant improvement over traditional altimetry. This study aims to compare data from the NOAA Global Drifter Program ($1^\circ \times 1^\circ$ resolution) and satellite products from AVISO Globcurrent ($1/4^\circ$ resolution) as well as SWOT KaRIn and nadir ($1/60^\circ$ resolution), by adjusting the non-geostrophic components of the currents as needed.

Inertial oscillations are obtained by filtering the drifter current data. We used three filtering methods : the linear Ubelmann filter, the non-linear median filter, and the linear Hanning filter, which provides the most consistent results. Indeed, tests show that the Hanning filter most improves the quality of surface currents from drifters, with a 14% improvement in the geostrophic component for the zonal component and 16% for the meridional component.

A spatial and then temporal sliding filter over different windows is also employed to filter small scales and high frequencies contained within SWOT data. SWOT data are consistent with large-scale CMEMS data after spatial filtering with a window of about 1° . Comparison with drifter buoys reveals that CMEMS poorly represents the variations in drifter currents. SWOT shows better correlation for zonal geostrophic currents, particularly after a 5-day temporal smoothing, but does not provide apparent improvement for the meridional component. This is interpreted as a result of the asymmetry of the SWOT trace, which is elongated in latitude and narrow in longitude. Therefore, spatial smoothing at 1° is problematic for zonal direction and meridional current estimation (which is derived from zonal differentiation). Simulations were performed using the Python programming language.

Keywords : Ocean circulation and dynamics, Lagrangian trajectory applications, Drifting buoys, Satellite products, Physical oceanography.

Contents

Dedication	i
Remerciements	ii
Résumé	iv
Abstract	v
Listes des figures	viii
1 Introduction	2
1 Problem Statement	3
2 Objectives and Goals	3
3 Justification of Objectives	3
4 Organization of the Study	3
2 Geostrophic and Ageostrophic Components of Currents	4
1 The Geostrophic Component	4
2 The Ageostrophic Components	5
2.1 The Ekman Component	6
2.2 The Inertial Component	6
3 Data and Methods	9
1 Data	9
1.1 Altimetric Data	9
1.2 Drifting Buoy Data	10
2 Methods	11
2.1 Evaluation of the Inertial Component	11
2.1.1 Nonlinear Median Filter	11
2.1.2 Linear Hanning Filter	11
2.1.3 Linear Ubelmann Filter	12
2.2 Tool Availability	13

2.3	Evaluation Diagnostic	13
4	Results, Analyses, and Discussions	15
1	Validation of Ocean Surface Currents from Globcurrent Products Using Drifter Data	15
1.1	Combined Analysis of Drifters: Eddy vs. Inertial Oscillations	15
1.1.1	Analysis of the Drifter with Eddy Characteristics	16
1.1.2	Analysis of the Drifter with Inertial Oscillations	19
2	Synthesis of Results for All Drifters	22
5	Contribution of the SWOT Satellite to the Study	24
1	Design and Objectives of the SWOT Satellite	24
2	Assessment Diagnostics	25
2.1	Comparison of AVISO Geostrophic Currents with Those from SWOT	26
2.2	Comparison of SWOT Geostrophic Currents and Global Drifter . .	27
3	Conclusion	29
6	Conclusion and Recommendations	30

List of Figures

3.1 Altimetric satellites: past, ongoing, and future missions (adapted from Taburet et al., 2019)	10
3.2 Geographic outline (dashed box) of the analysis region. Drifter trajectories from January 2019 to December 2023 were used for computing drifter velocities in the analysis. The number of drifters is 967.	14
3.3 Position of the drifters on 2019-01-01 06:00:00	14
4.1 Zonal and meridional currents of the drifter (a, c), interpolated geostrophic currents from Aviso (b, d), SSH distribution and drifter position (e, f), SST distribution (g).	17
4.2 Comparison of speeds derived from drifters and satellites: time series (a, c) and analysis of correlation, regression, and RMSE (b, d).	18
4.3 Statistical comparison of speeds derived from drifters and satellites for (a) zonal currents and (b) meridional currents.	18
4.4 Zonal and meridional currents of the drifter (a, c), interpolated geostrophic currents from Aviso (b, d), SSH distribution and position of the drifter (e, f), SST distribution (g).	20
4.5 Statistical comparison of speeds derived from drifters and satellites for (a, c) zonal currents and (b, d) meridional currents.	21
4.6 Zonal and meridional currents of drifters (a, b), interpolated geostrophic currents from Aviso (c, d).	22
4.7 Initial inertial speed: zonal u_0 in (blue) and meridional v_0 in (red).	23
5.1 Measurement principle of the SWOT satellite. Credits: NASA-JPL	24
5.2 Projection of SWOT sea surface height (SSH) in the tropical Atlantic (a) and an overview of its track (b).	25
5.3 Interpolation of SWOT and AVISO geostrophic currents on the SWOT grid: Zonal case (a, b) and meridional case (c, d).	26
5.4 Statistical analysis of spatial correlations between the interpolated geostrophic currents from SWOT and AVISO: Zonal case (a) and meridional case (b).	27

5.5	SWOT trace for April 2, 2023, and the trajectory of the drifters.	28
5.6	Trajectory of the drifters superimposed on the meridional velocity fields of SWOT and CMEMS.	28
5.7	Time series analysis between geostrophic currents from CMEMS and Drifter currents: Zonal case (a) and Meridional case (b).	29
5.8	Time series analysis between SWOT geostrophic currents and Drifter currents: Zonal case (a) and Meridional case (b).	29

LIST OF ABBREVIATIONS

JPL :	Jet Propulsion Laboratory
KaRIn :	Ka-band Radar Interferometer
SWOT :	Surface Water Ocean Topography
SAR :	Synthetic Aperture Radar
DUACS :		Data Unification and Altimeter Combination System
CMEMS :		Copernicus Marine Environment Monitoring Service
NOAA :	.	National Ocean and Atmospheric Administration
u :	Zonal speed of the drifter
v :	Meridional speed of the drifter
ue :	Zonal Ekman current
ve :	Meridional Ekman current
ui :	Zonal inertial current
vi :	Meridional inertial current
SSH :	Sea Surface Height
ugeos :	Zonal geostrophic current
vgeos :	Meridional geostrophic current

Introduction

Surface currents in oceanic environments play a fundamental role in the transport of energy, heat, salt, and various tracers over vast distances. Their dynamics influence climatic conditions, the dispersion of floating materials, the management of marine resources, as well as the spread of pollutants. Traditionally, the estimation of ocean currents relied on ship drift, a method limited by coarse spatiotemporal sampling ([Richardson1989](#)). Since 1978, the introduction of satellite-tracked drifting buoys, as part of the NOAA Global Drifter Program, has significantly improved the assessment of ocean currents on a global scale ([Niiler2003](#), [LumpkinPazos2007](#)).

With the advent of newer technologies, such as extensive drifter databases and next-generation satellites like SWOT (Surface Water Ocean Topography), our understanding of ocean currents has further enriched. Satellite observations, particularly through AVISO's Globcurrent products and data from the CMEMS program, have transformed our analysis of ocean currents by providing a more detailed view of their dynamics and interaction with the global climate ([Picaut1990](#), [Lagerloef1999](#), [Sudre2013](#)). However, the precise characterization of ageostrophic currents at scales below 50 km, essential for understanding regional mechanisms, remains a challenge ([DohanMaximenko2010](#)).

To fill these gaps, this study focuses on the tropical Atlantic by combining data from the Global Drifter Program, Globcurrent satellite products, and high-precision measurements provided by the SWOT satellite, launched in 2022. The objective is to compare geostrophic and ageostrophic currents measured by these different sources, using appropriate filtering methods to analyze inertial oscillations and spatiotemporal variations. This approach aims to refine our understanding of ocean currents at fine scales (mesoscale and sub-mesoscale, [Wang et al., 2019](#)) and assess the improvements brought by new technologies compared to traditional satellite altimetry methods.

1.1 Problem Statement

Ocean surface currents, crucial for climate, marine ecosystems, and human activities, pose challenges of spatial and temporal sampling. The precise characterization of small-scale currents (10-50 km) is limited ([Picaut et al., 1990](#); [Lagerloef et al., 1999](#)), impacting our understanding of their variability, particularly in key regions like the tropical Atlantic.

1.2 Objectives and Goals

The main objective of this study is to confront currents derived from buoys with those from global products distributed by CMEMS or those derived from altimetry. To this end, we set the following specific objectives:

- Evaluate the accuracy of CMEMS global products by comparing them to currents measured by buoys.
- Assess the contribution of the SWOT satellite compared to traditional altimetry.

1.3 Justification of Objectives

Achieving these objectives will not only fill current gaps in the understanding of small-scale ocean currents but also provide crucial information to improve ocean forecasting models and climate predictions. Better characterization of ageostrophic currents will contribute to effective management of marine resources and enhanced assessment of environmental impacts.

1.4 Organization of the Study

This research document is organized into six chapters. Chapter two provides a general description of the geostrophic and ageostrophic components of marine currents as well as classical assessment methods and their limitations. The third chapter details the methodology employed to verify the accuracy of these components. The results obtained will be presented and discussed in the fourth and fifth chapters, while the sixth chapter will conclude our research thesis by summarizing the main findings, discussing implications, and suggesting directions for future research.

Geostrophic and Ageostrophic Components of Currents

This chapter aims to describe the different components of ocean currents, classifying them into two main categories: geostrophic currents and ageostrophic currents. Ageostrophic currents include phenomena such as the Ekman effect and inertial oscillations. Marine currents can thus be decomposed into zonal and meridional currents (u, v), which result from the sum of the geostrophic components (u_g, v_g), Ekman components (u_e, v_e), and inertial components (u_i, v_i).

To analyze these components, we use the equations of motion formulated by [Bougeault and Sadourny \(2001\)](#). Considering a frame of reference linked to the Earth (i.e., rotating with the axis z representing the vertical), and assuming a homogeneous and stationary fluid, the equations of conservation of momentum are as follows:

$$\frac{\partial \mathbf{u}}{\partial t} + (\mathbf{u} \cdot \nabla) \mathbf{u} = -\frac{1}{\rho} \nabla p + \mathbf{f}_{\text{cor}} + \nu \nabla^2 \mathbf{u} \quad (2.1)$$

where \mathbf{u} is the current velocity, ρ is the fluid density, p is the pressure, \mathbf{f}_{cor} is the Coriolis force, and ν is the viscosity. The equation of conservation of mass for an incompressible fluid is given by:

$$\nabla \cdot \mathbf{u} = 0 \quad (2.2)$$

These equations allow modeling and understanding the different types of ocean currents while accounting for geostrophic and ageostrophic effects.

2.1 The Geostrophic Component

The geostrophic balance, which assumes weak advection of momentum and friction forces, provides the geostrophic velocities u_g and v_g outside the equatorial band, where

the Coriolis force is zero. The geostrophic equations are:

$$u_g = -\frac{g}{f} \frac{\partial h}{\partial y} \quad (2.3)$$

$$v_g = \frac{g}{f} \frac{\partial h}{\partial x} \quad (2.4)$$

where f is the Coriolis parameter, g is the acceleration due to gravity (9.807 m/s^2), h is the map of absolute dynamic topography (MADT), and y and x are the positions in latitude and longitude. These data come from the Data Unification and Altimeter Combination System AVISO (www.aviso.oceanobs.com/en/data/productsinformation/duacs) with a resolution of $1/3^\circ$ in Mercator grid.

At the equator, where $f = 0$, the geostrophic equations become singular. [Moore and Philander \(1978\)](#) recommend using the second derivative of the meridional pressure field with $f = by$, where b is a constant. The equations for semi-geostrophic currents u_{sg} and v_{sg} are:

$$u_{sg} = -\frac{g}{\beta} \frac{\partial^2 h}{\partial y^2} \quad (2.5)$$

$$v_{sg} = \frac{g}{\beta} \frac{\partial^2 h}{\partial x^2} \quad (2.6)$$

where $\beta = 2.3 \times 10^{-11} \text{ m}^{-1} \text{ s}^{-1}$. To use these equations, the first meridional derivative of h must be zero, necessitating a correction factor in the MADT ([Picaut and Tournier, 1991](#)). Continuity between the geostrophic and semi-geostrophic regimes is ensured by a spline function in the band 28°N – 28°S , while outside this zone, currents remain geostrophic.

2.2 The Ageostrophic Components

The ageostrophic components of currents emerge when the ideal conditions of geostrophic motion, characterized by a balance between the Coriolis force and the pressure gradient, are disturbed by external influences such as friction, density variations, and non-geostrophic forces. These disturbances modify the speed, direction, and trajectory of currents relative to geostrophic forecasts, which are crucial for heat and material transport.

By isolating the ageostrophic effects, we can express the ageostrophic components of

marine currents as:

$$\mathbf{u}_{\text{ageos}} = \mathbf{u} - \mathbf{u}_{\text{geos}} \quad (2.7)$$

where \mathbf{u}_{geos} is the current speed calculated from the geostrophic solution, and $\mathbf{u}_{\text{ageos}}$ represents the ageostrophic deviations defined as follows:

2.2.1 The Ekman Component

The Ekman model, based on the work of [van Meurs and Niiler \(1997\)](#) and [Lagerloef et al. \(1999\)](#), describes the linear momentum balance for wind-driven current with the following equations:

$$fh_e u_e + r_e v_e = \frac{\tau_y}{\rho} \quad (2.8)$$

$$r_e u_e - fh_e v_e = \frac{\tau_x}{\rho} \quad (2.9)$$

where $\tau = (\tau_x, \tau_y)$ is the wind stress field, $\rho = 1025 \text{ kg/m}^3$ is the density of water, and h_e and r_e are respectively the thickness of the Ekman layer and the linear drag coefficient. These parameters must be estimated before determining the Ekman current, but they are often unknown in the real ocean. [Lagerloef et al. \(1999\)](#) derived (h_e, r_e) by a constant linear regression, while [Sudre and Morrow \(2008\)](#) suggested an improvement to account for the variability of h_e . [Sudre \(2013\)](#) attempted to estimate these parameters from surface drifter observations, but the Earth's rotation and inertial forces add additional complexities to the improvement of surface current models ([Liu et al., 2022](#)).

2.2.2 The Inertial Component

The inertial regression model of the current, according to [Durrant \(1993\)](#), is based on the following equations for the stable linear momentum balance:

$$\frac{\partial v}{\partial t} + fu = \frac{1}{\rho} \frac{\partial p}{\partial y} \quad (2.10)$$

$$\frac{\partial u}{\partial t} - fv = -\frac{1}{\rho} \frac{\partial p}{\partial x} \quad (2.11)$$

where p is the pressure, ρ is the density, and u and v are the components of wind speed

in Cartesian coordinates with x being east-west ([Holton 1992, p. 40](#)). As in the classical "f-plane" approximation, let us assume f is constant and vertical motions are neglected; inertial oscillation occurs when pressure gradients are zero:

$$\frac{du}{dt} - fv = 0 \quad (2.12)$$

$$\frac{dv}{dt} + fu = 0 \quad (2.13)$$

By differentiating the first equation with respect to time and using the second, we obtain:

$$\frac{du}{dt} + fu = 0 \quad (2.14)$$

which has sinusoidal solutions with a period $\frac{2\pi}{f}$. With $u = u_0$ and $v = 0$ at $t = 0$, the subsequent speeds are:

$$u_i(t) = u_0 \cos(ft) \quad (2.15)$$

$$v_i(t) = u_0 \sin(ft) \quad (2.16)$$

An air parcel follows a circular inertial trajectory:

$$x(t) = \frac{u_0}{f} \sin(ft) \quad (2.17)$$

$$y(t) = -\frac{u_0}{f} \cos(ft) \quad (2.18)$$

The radius of curvature for an anticyclonic displacement is $\frac{u_0}{f}$. Gravity also influences the inertial oscillation [Durran \(1993\)](#). Details on estimating this component will be provided in the Method section of Chapter 3.

In conclusion, this chapter has clarified the different components of ocean currents by distinguishing geostrophic currents, resulting from the balance between the Coriolis force and the pressure gradient, from ageostrophic currents, influenced by phenomena such as the Ekman effect and inertial oscillations. By using advanced models and conservation equations, we studied how these currents interact, which is crucial for improving ocean forecasts and applications.

However, precisely evaluating these different measured components is complex due to the limitations of classical methods like numerical models and direct observations. Drifting buoys provide accurate but geographically limited data, while satellite altimetry covers vast areas but sometimes lacks precision. The SWOT satellite provides highly accurate estimates of geostrophic currents. An effective solution is to combine detailed buoy data with the extensive coverage of satellite products ([Sudre et al., 2013](#)).

Data and Methods

“Whoever perseveres in their research is eventually led to change their methods”

J. W. Goethe

In this chapter, we describe the main data utilized during this research thesis as well as the various methods employed. The data primarily consist of satellite observations and in-situ data, including sea surface heights and anomalies, sea surface temperature, as well as geostrophic, Ekman, and total currents measured by drifting buoys.

3.1 Data

3.1.1 Altimetric Data

Satellite altimetry measures and maps the topography of the oceans with global coverage. It was launched with Geos-3 in 1975 and developed with Topex/Poseidon in 1992 by NASA and CNES. This technique provides a resolution of 0.25° and 1 day. Since then, more advanced satellites have improved the accuracy of measurements and their integration into climate models (Dufau et al., 2016; Hermozo, 2018).

Figure 3-1 presents past and future altimetric missions, including the SWOT mission, launched in late 2022, which provides high-resolution data on ocean and continental water levels. Altimetric measurement uses radar waves to determine the distance between a satellite and the sea surface, allowing for the estimation of sea surface height (SSH) and absolute dynamic topography (ADT) relative to the geoid, thus replacing the reference ellipsoid. SSH is calculated by subtracting the measured distance from the satellite's altitude.

In my research, I use altimetry data, including sea level anomaly (SLA), sea surface temperature (SST), geostrophic currents zonal (u_{geos}) and meridional (v_{geos}), as well as the zonal and meridional components of the Ekman current (u_e and v_e). These data, provided freely by the CMEMS service, are interpolated onto a regular grid of 0.25° in

longitude/latitude and updated daily. For analyzing sea level anomalies and geostrophic currents (2019-2023), we utilize the Globcurrent product from AVISO. The SST data come from the MULTIOBS product. Additionally, data from the SWOT satellite from the NRT SWOT KaRIn & nadir product (1/60° grid, March-July 2023) are also used.

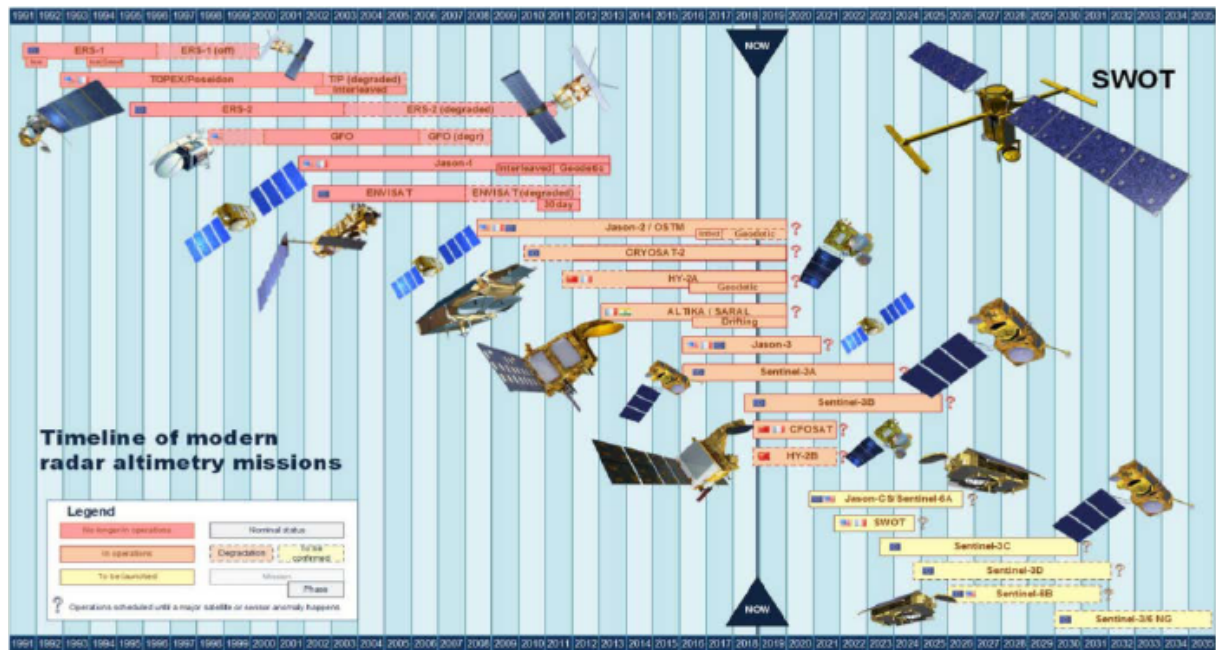


Figure 3.1 – Altimetric satellites: past, ongoing, and future missions (adapted from Taburet et al., 2019)

3.1.2 Drifting Buoy Data



Figure 3.1 – Photos of a drifting buoy (Bourlès et al., 1999a, page 98). The subsurface drogue is positioned at approximately 15m depth. Data is transmitted daily via the Argos satellite transmission system.

In this research, I use drifter data (zonal current v_e and meridional current v_n), provided by NOAA. These data have a temporal resolution of 6 hours and a spatial resolution of $1^\circ \times 1^\circ$, covering the period from 2019 to 2023 and are available daily through the Global Drifter Program. [Figure 3.2](#) presents a photo of a drifter. Drifters measure ocean currents by moving with them and recording variations in their position.

3.2 Methods

3.2.1 Evaluation of the Inertial Component

The inertial component of the currents measured by the drifting buoys is extracted from the data using three specific types of filters: the [nonlinear median filter](#), the [linear Hanning filter](#), and the [linear Ubelmann filter](#).

3.2.1.1 Nonlinear Median Filter

The nonlinear median filter is particularly useful for processing the time series of current components from the drifters, reducing noise while preserving significant variations. Let $x(t)$ be the time series of current components measured by a drifter. The median filter replaces each value $x(t_i)$ with the median of the values in a time window around t_i . Mathematically, for a time window of size $2k + 1$ centered at t_i , the filtered value $x'(t_i)$ is given by:

$$x'(t_i) = \text{Median}(x(t_{i-k}), x(t_{i-k+1}), \dots, x(t_{i+k}))$$

where Median denotes the function that calculates the median of the values within the time window. The choice of window size $2k + 1$ is crucial: a larger window may better eliminate noise but can also smooth out the actual variations in currents. Conversely, a smaller window preserves finer details but may not effectively remove noise. This filter is therefore suitable for removing anomalies while preserving the fundamental variations of the measured current.

3.2.1.2 Linear Hanning Filter

The linear Hanning filter is particularly useful in processing the time series of current components from the drifters. This filter smooths transitions in the data by averaging

values and reducing sharp variations. This process improves the accuracy of frequency analysis by eliminating unwanted high-frequency components.

Mathematically, the Hanning filter is applied to a time series $x(t)$ using a window function defined for a window size N . The Hanning window function $w(t)$ is given by:

$$w(t) = 0.5 \left(1 - \cos\left(\frac{2\pi t}{N-1}\right)\right)$$

where t varies from 0 to $N - 1$. To apply the filter, each value $x(t_i)$ of the time series is multiplied by the corresponding value of the window function $w(t_i)$:

$$x'(t_i) = x(t_i) \cdot w(t_i)$$

Thus, the Hanning filter improves the quality of frequency analyses by removing unwanted noise components and facilitating the interpretation of the actual variations of the measured currents.

3.2.1.3 Linear Ubelmann Filter

The linear Ubelmann filter, specifically designed for this research, is a convolution filter that uses an impulse response tailored to the inertial characteristics of the currents to effectively isolate the inertial component based on the Coriolis frequency f_c . The time parameter of the filter is:

$$\tau_l = \frac{3}{f_c}$$

The filter is defined as:

$$g(t) = e^{-if_ct} \cdot e^{-\left(\frac{t}{\tau_l}\right)^2}$$

and is normalized so that the sum of the absolute values equals 1:

$$g_{\text{normalized}}(t) = \frac{g(t)}{\sum_t |g(t)|}$$

It is applied to the complex signal U (composed of the u and v velocities) by convolution:

$$U_{\text{filtered}}(t) = (U * g)(t)$$

where $*$ represents the convolution between the signal U and the filter $g(t)$.

3.2.2 Tool Availability

For our analysis, we used Python 3.5 for computations and GitHub for collaboration and documentation of the code. Links to the GitHub code and data from the NOAA Global Drifter Program, SWOT, AVISO's Globcurrent, as well as SST data are provided respectively by:

1. <https://github.com/Julio-Leonel-Donfack>;
2. https://erddap.aoml.noaa.gov/gdp/erddap/tabledap/drifter_6hour_qc.html;
3. <https://filesender.renater.fr/?s=download&token=b80bdfdb-2153-421d-86af-dc3849c1>
4. https://data.marine.copernicus.eu/product/MULTIOBS_GLO_PHY_MYNRT_015_003/download
5. https://data.marine.copernicus.eu/product/MULTIOBS_GLO_PHY_SSS_L4_MY_015_015_015/download.

3.2.3 Evaluation Diagnostic

To evaluate ocean surface currents, we used 967 drifters from the NOAA Global Drifter Program. The trajectories of these drifters, shown in [Figure 4.1](#), reveal a daily distribution of about sixty units, with positions varying each day, as illustrated in [Figure 4.2](#).

The drifters are mostly influenced by inertial effects (91.42%) and, to a lesser extent, by vortices. The inertial period is given by $T = \frac{2\pi}{f}$ with $f = 2\Omega \sin(\phi)$, where Ω is the Earth's angular velocity and ϕ is the latitude. Vortices are detected by a two-step algorithm: localization of the center (maximum or minimum of SLA/ADT) and delimitation of the edge (closed contour around the center) ([Chaigneau2008](#), [Chaigneau2009](#), [Pegliasco2015](#), [Assassi et al., 2016](#)).

Initial analyses were conducted on two drifters and then extended to all drifters for an overview. To compare geostrophic currents with drifter data, geostrophic currents from the Globcurrent product were adjusted and interpolated to match the positions of the drifters. These geostrophic currents were then combined with the Ekman components provided by Globcurrent, and the inertial oscillations were filtered from the drifter current components.

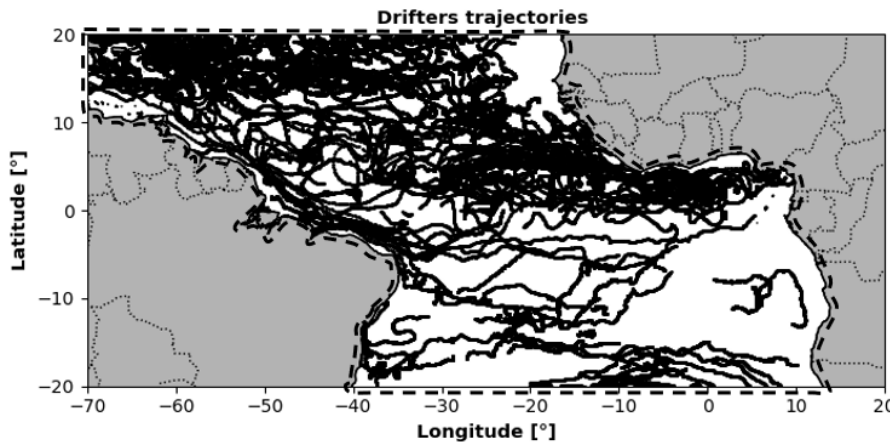


Figure 3.2 – Geographic outline (dashed box) of the analysis region. Drifter trajectories from January 2019 to December 2023 were used for computing drifter velocities in the analysis. The number of drifters is 967.

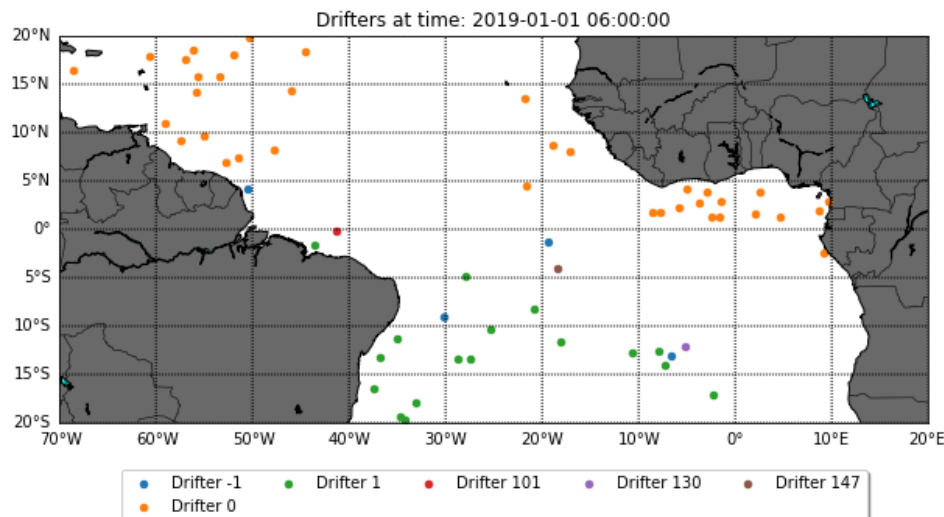


Figure 3.3 – Position of the drifters on 2019-01-01 06:00:00

Finally, we compared the combined currents (geostrophic plus Ekman) from the Globcurrent product with the filtered currents from the drifters to assess their concordance using statistical tests, such as calculating the Pearson correlation coefficient, directional coefficient, and root mean square error (RMSE), whose expressions are respectively given by:

$$\text{RMSE} = \sqrt{\frac{1}{N} \sum_{i=1}^N (x_i - \hat{x}_i)^2}$$

$$r = \frac{N \sum (x_i \hat{x}_i) - (\sum x_i)(\sum \hat{x}_i)}{\sqrt{\left[N \sum x_i^2 - (\sum x_i)^2 \right] \left[N \sum \hat{x}_i^2 - (\sum \hat{x}_i)^2 \right]}} ; \quad b = \frac{N \sum (x_i \hat{x}_i) - (\sum x_i)(\sum \hat{x}_i)}{N \sum x_i^2 - (\sum x_i)^2}$$

Where x_i is the data from the drifting buoys, \hat{x}_i is that from the satellite products, N is the number of pixels, and i is the pixel index.

Results, Analyses, and Discussions

"Scientific discoveries remind us that the world is full of mysteries to explore, and that each result opens the way to a new understanding."

Albert Einstein

In this chapter, we examine the first part of the research results, evaluating the quality of ocean surface currents from satellite products using the "AVISO" data from the DUACS system, available through the Copernicus Marine Service (CMEMS). The contribution of the SWOT satellite will be addressed in [Chapter 5](#). Drifting buoys, particularly the NOAA's Global Drifter Program drifters, are used to validate satellite product observations.

4.1 Validation of Ocean Surface Currents from Globcurrent Products Using Drifter Data

Although eddies and inertial oscillations are both related to fluid dynamics and the Earth's rotation, they differ in their periods. The period of inertial oscillations is $\frac{2\pi}{f}$, where f is the Coriolis frequency ([Susan et al., 2005; Persson, A., 2005](#)), while eddies do not have a defined unique period and exhibit more complex dynamics. In the following sections, we will apply a combined analysis on two drifters: one with eddy characteristics and the other with inertial oscillations, followed by a synthesis for all the drifters.

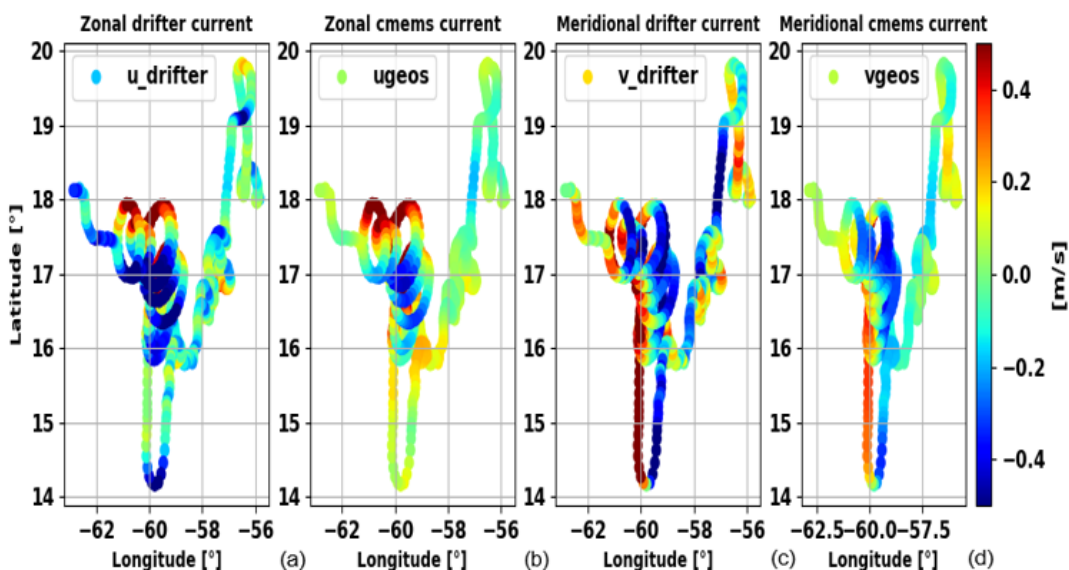
4.1.1 Combined Analysis of Drifters: Eddy vs. Inertial Oscillations

4.1.1.1 Analysis of the Drifter with Eddy Characteristics

The selected drifter is influenced by a current associated with an eddy throughout its trajectory, with a total of 813 observations collected. The visualization of its trajectories over SSH and SST fields revealed a surface anticyclonic eddy, as described by Chaigneau et al. (2008) and Assassi et al. (2016). Indeed, the drifter is located in a concave area of the SSH field, with a surface temperature of about 27°C, confirming the presence of the eddy. This eddy, influenced by the Caribbean current, has an amplitude of 1.5 m, a radius of 13 to 40 km, and a kinetic energy of 30 m²/s².

Figure 4.1 shows that the currents measured by CMEMS are generally consistent with those of the drifter, but exhibit lower intensities. This difference is partly due to CMEMS's limited spatial resolution of 1/4°, as well as the absence of ageostrophic components in the currents provided by CMEMS. Furthermore, the negative intensity of the observed currents is attributed to the drifter's location in a westward current zone, considered negative (Bourlet et al., 2008).

To improve the quality of the currents observed by satellite products, we added the Ekman components to the zonal and meridional components. Figure 4.2 illustrates this correction. Since the currents measured by the drifter include eddies, we used three filters for extraction, with the Hanning linear filter yielding the most consistent results. The results are shown in Figure 4.3, and the evaluation of the analyses is presented in Table 4.1.



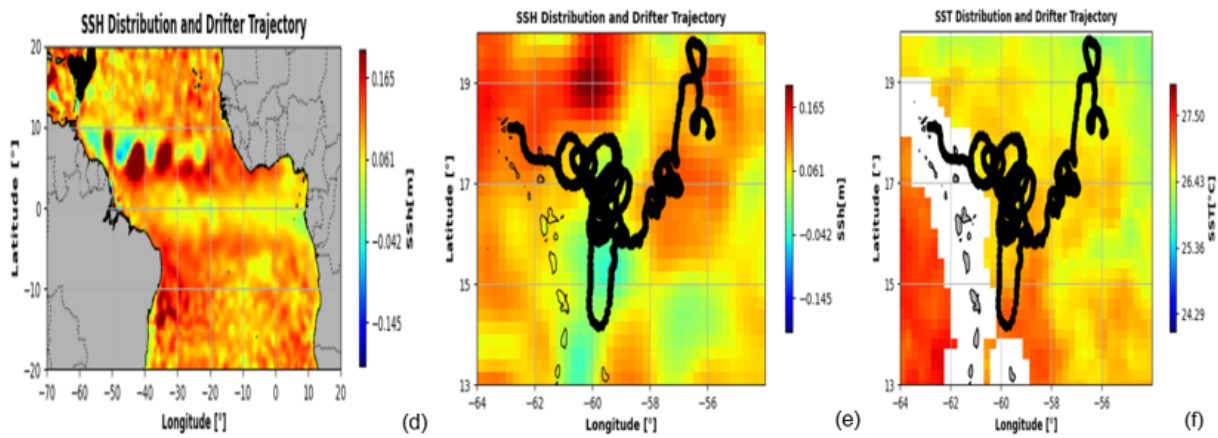
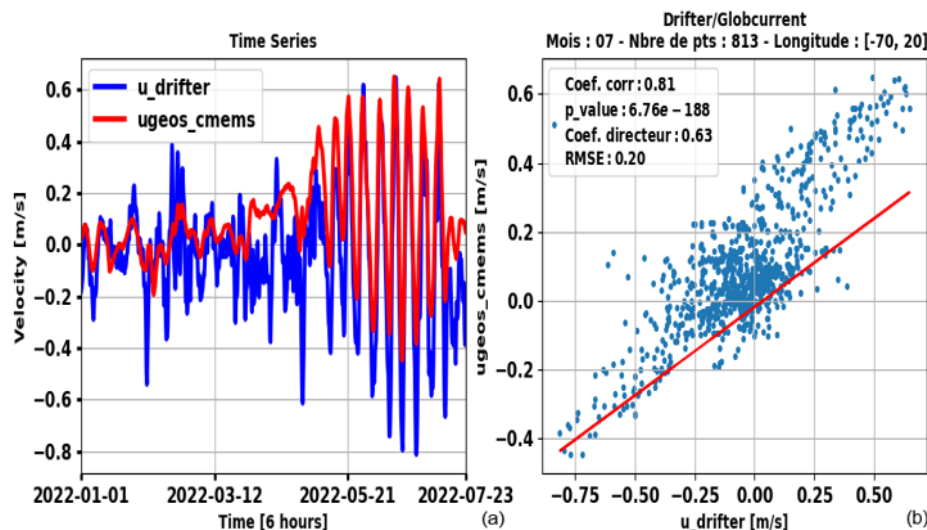


Figure 4.1 – Zonal and meridional currents of the drifter (a, c), interpolated geostrophic currents from Aviso (b, d), SSH distribution and drifter position (e, f), SST distribution (g).

Figure 4.2 shows that the currents measured by the Global Drifter Program drifters are strongly correlated with the geostrophic currents from Globcurrent, with correlation coefficients of 0.81 for zonal and 0.82 for meridional currents, and very low p-values. The regression coefficients are 0.63 for zonal and 0.52 for meridional, while the RMSE values are 0.20 m/s for zonal and 0.16 m/s for meridional.

These results indicate that geostrophic models accurately predict the measured currents, although they do not account for all current components. After integrating the Ekman current and applying the Hanning filter, the statistics show a significant improvement. The forecasts for the zonal current have a correlation of 0.81, with a low p-value and an RMSE of 0.14 m/s. For the meridional current, the correlation is 0.87, also with a low p-value and an RMSE of 0.11 m/s.



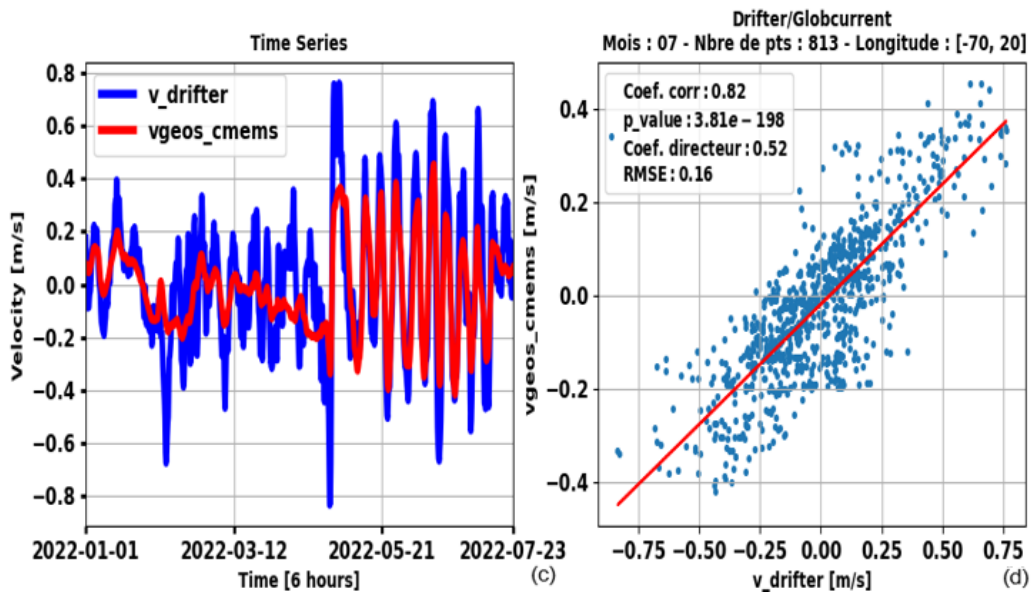


Figure 4.2 – Comparison of speeds derived from drifters and satellites: time series (a, c) and analysis of correlation, regression, and RMSE (b, d).

In summary, these adjustments have significantly improved the accuracy of the forecasts, especially for the meridional currents (see Figure 4.3).

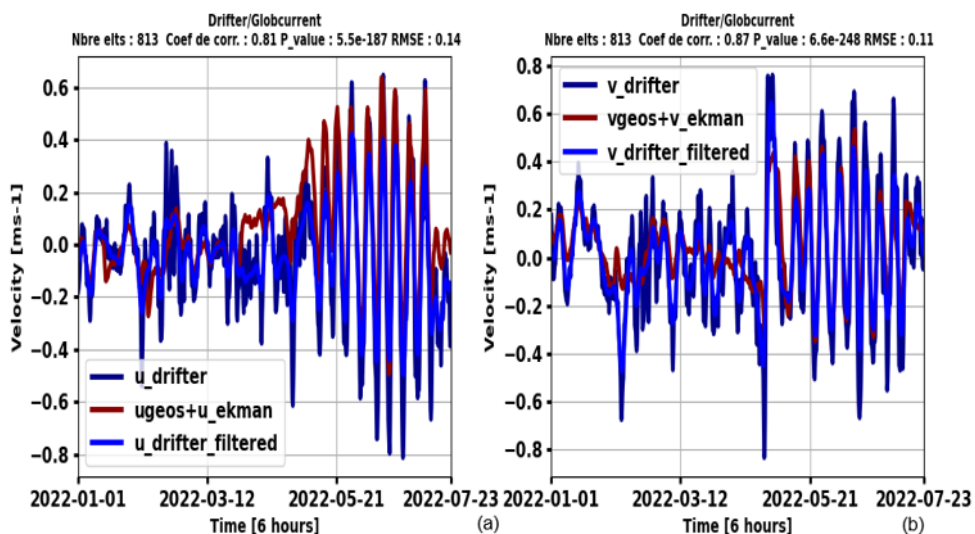


Figure 4.3 – Statistical comparison of speeds derived from drifters and satellites for (a) zonal currents and (b) meridional currents.

The filters used in this section, although designed to eliminate inertial frequencies, are particularly effective at attenuating eddies and other disturbances in the drifter speed data. They reduce high frequencies while preserving significant low-frequency components, thereby improving data quality and allowing for a more accurate analysis of oceanic movements.

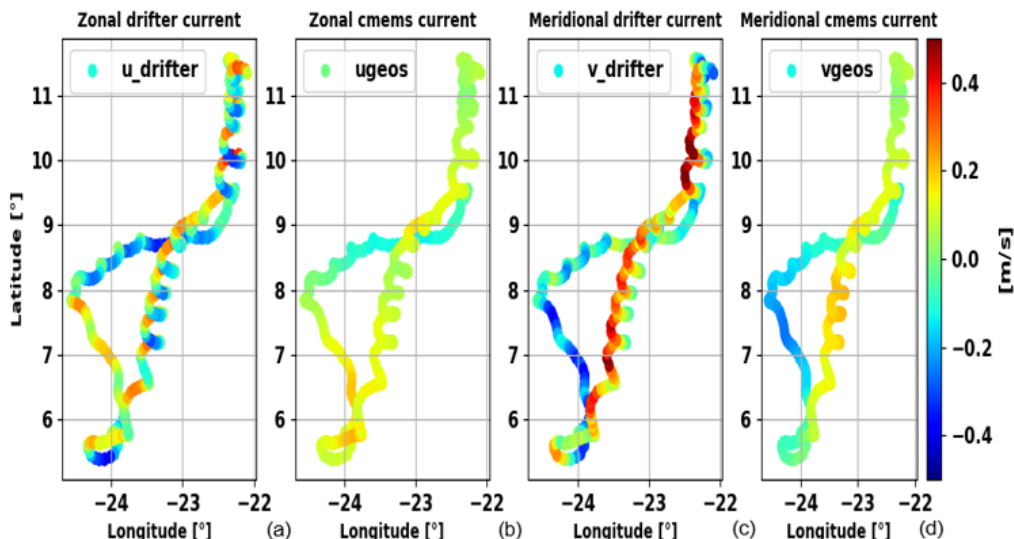
Table 4.1 – Table comparing surface speeds from Glocurrent to the speeds of a drifter taken in a vortex at 15 m in the region 20°N-20°S and 70°W-20°E.

Variables	Corr. Coef.	P-value	Regression Coef.	RMSE
(ugeos, u-drifter)	0.81	6.76e-188	0.63	0.20
(vgeos, v-drifter)	0.82	3.81e-198	0.52	0.16
(ugos+ue, u-drifter)	0.81	4.29e-186	0.64	0.17
(vgeos+ve, v-drifter)	0.84	4.24e-215	0.53	0.16
(ugeos+ue, Hanning filter u-filtered)	0.81	5.51e-187	0.64	0.14
Clemem filter	0.00	0.92	-1.54	4401
Median filter	0.81	1.03	0.65	0.17
(vgeos+ve, Hanning filter v-filtered)	0.87	6.59e-248	0.75	0.11
Clemem filter	-0.03	0.47	-6.87	6243
Median filter	0.84	5.97	0.53	0.16

In conclusion, Table 4.1 shows that the surface speeds measured by Glocurrent and those from NOAA at 15 meters for our drifter between 20°N-20°S and 70°W-20°E are better aligned with filtered data. Models combining geostrophy and Ekman effects, and using filters, provide better correlation and accuracy. The linear Hanning filter performs the best with a correlation of 0.87 and an RMSE of 0.11, while the linear Ubelmann and nonlinear Median filters show more variable results.

4.1.1.2 Analysis of the Drifter with Inertial Oscillations

The selected drifter is influenced by a current associated with inertia throughout its trajectory, with a total of 404 observations collected. Its inertial period, calculated at



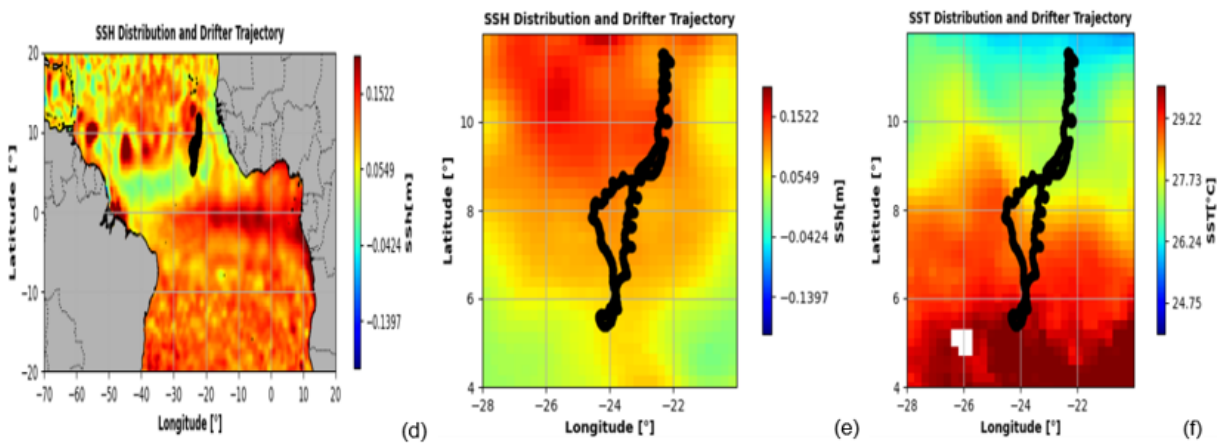
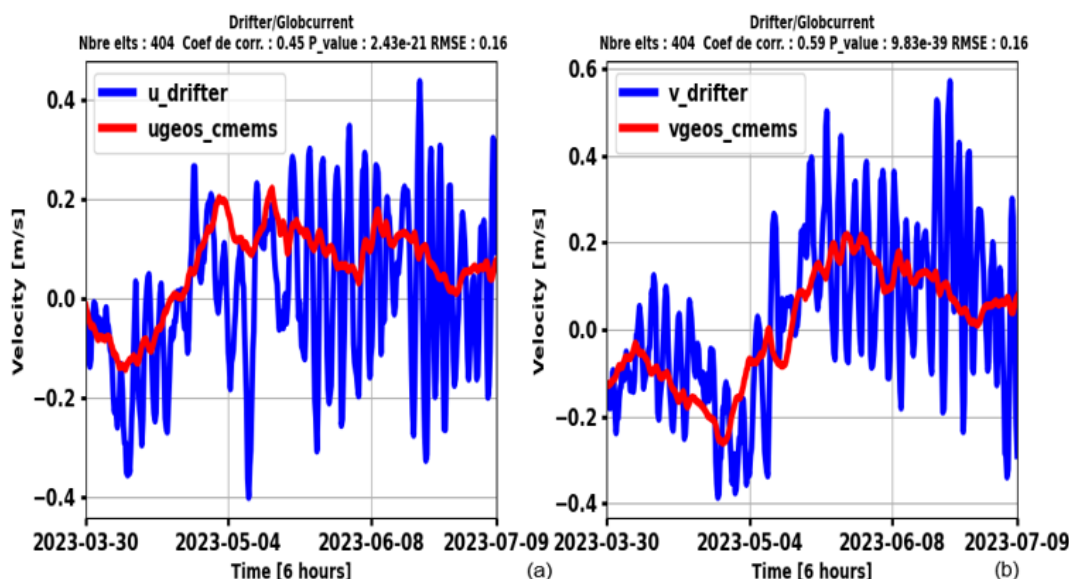


Figure 4.4 – Zonal and meridional currents of the drifter (a, c), interpolated geostrophic currents from Aviso (b, d), SSH distribution and position of the drifter (e, f), SST distribution (g).

86 hours, matches the measurements obtained by FFT ([Susan et al., 2005](#); [Persson, A., 2005](#)). The trajectory of the drifter shows a concentration of SSH along the diameter of the vortex, as indicated in [Figure 4.4-\(b\)](#), confirming the influence of inertial components on the currents measured by the drifters.

[Figure 4.4](#) shows that, although the currents measured by CMEMS are consistent with those of the drifters, their intensity is lower. This difference is partly due to the additional components of the drifter currents, such as Ekman, inertial, and cyclogeostrophic effects, as well as the limited spatial resolution of CMEMS, which is $1/4^\circ$. Furthermore, the positive intensity observed is attributed to the drifter's presence in an area of eastward currents, considered positive ([Bourlet et al., 2008](#)).



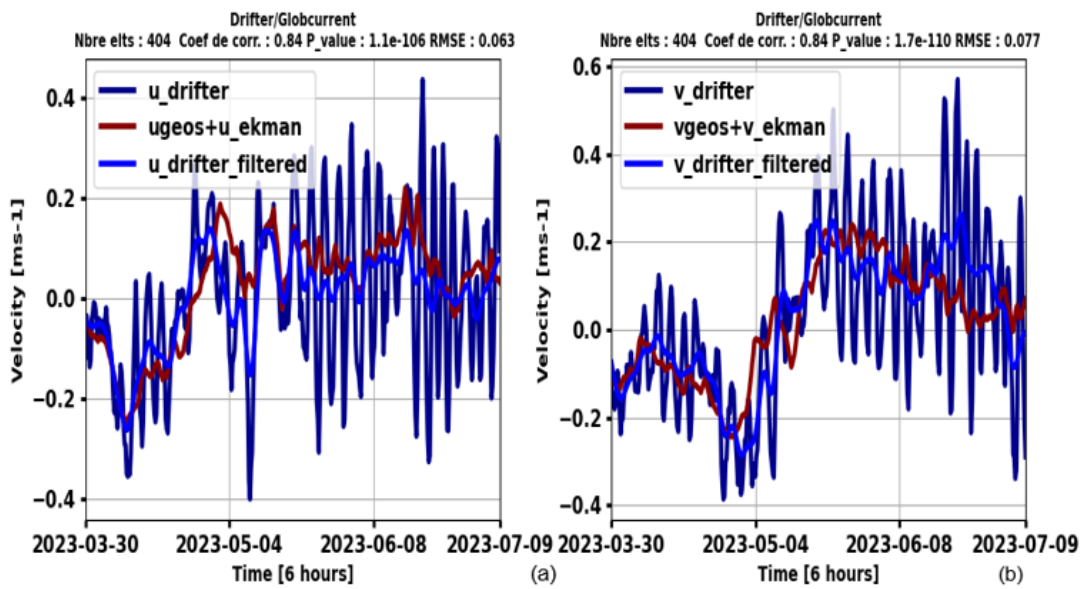


Figure 4.5 – Statistical comparison of speeds derived from drifters and satellites for (a, c) zonal currents and (b, d) meridional currents.

To improve the accuracy of the currents measured by satellite, we incorporated Ekman components into the zonal and meridional components. The currents obtained from the drifter, taking into account inertia, were filtered using three types of filters, including a Ubelmann linear filter, which proved as effective as the Hanning filter in smoothing the data and minimizing spectral leakage. The results and analyses are illustrated in [Figure 4.7](#) and [Table 4.2](#).

Table 4.2 – Table comparing surface speeds from Globcurrent to the speeds of a drifter subject to inertial oscillations at 15 m in the region 20°N-20°S and 70°W-20°E.

Variables	Corr. Coef.	P-value	Regression Coef.	RMSE
(ugeos, u-drifter)	0.45	4.3e-21	0.25	0.16
(vgeos, v-drifter)	0.59	9.83e-39	0.38	0.16
(ugeos+ue, u-drifter)	0.47	4.41e-23	0.31	0.15
(vgeos+ve, v-drifter)	0.60	1.84e-40	0.38	0.16
(ugeos+ue, Hanning filter u-filtered)	0.84	1.05e-106	1.00	0.063
Clemem filter	0.83	2.47e-104	1.74	0.073
Median filter	0.48	1.57	0.32	0.14
(vgeos+ve, Hanning filter v-filtered)	0.84	1.66e-110	0.75	0.077
Clemem filter	0.83	1.08e-105	1.34	0.076
Median filter	0.61	5.15	0.40	0.16

In conclusion, [Table 4.2](#) shows that the components of the speeds measured by the

Globcurrent product align better with those of NOAA when using Hanning and Clemem filters, with correlation coefficients of 0.84 and low RMSE (0.063 and 0.077, respectively). The nonlinear median filter yields less consistent results with lower correlation coefficients (0.48 and 0.61) and higher RMSE (0.14 and 0.16). Adjustments for Ekman effects improve accuracy, particularly when combined with Hanning and Ubelmann filters.

4.2 Synthesis of Results for All Drifters

In this section, we apply the combined analysis method to our 967 drifters over a period of 5 years. Figure 4.6 illustrates that the currents measured by CMEMS are consistent with those of the drifters, but their intensity remains lower due to ageostrophic effects on the drifters and the limited spatial resolution of CMEMS ($1/4^\circ$). The predominance of negative intensity currents is linked to the dominant westward currents in the tropical Atlantic, considered negative (Bourlet et al., 2008). The initial speeds of the inertial components are shown in Figure 4.7, and the overall conclusions are summarized in Table 4.3.

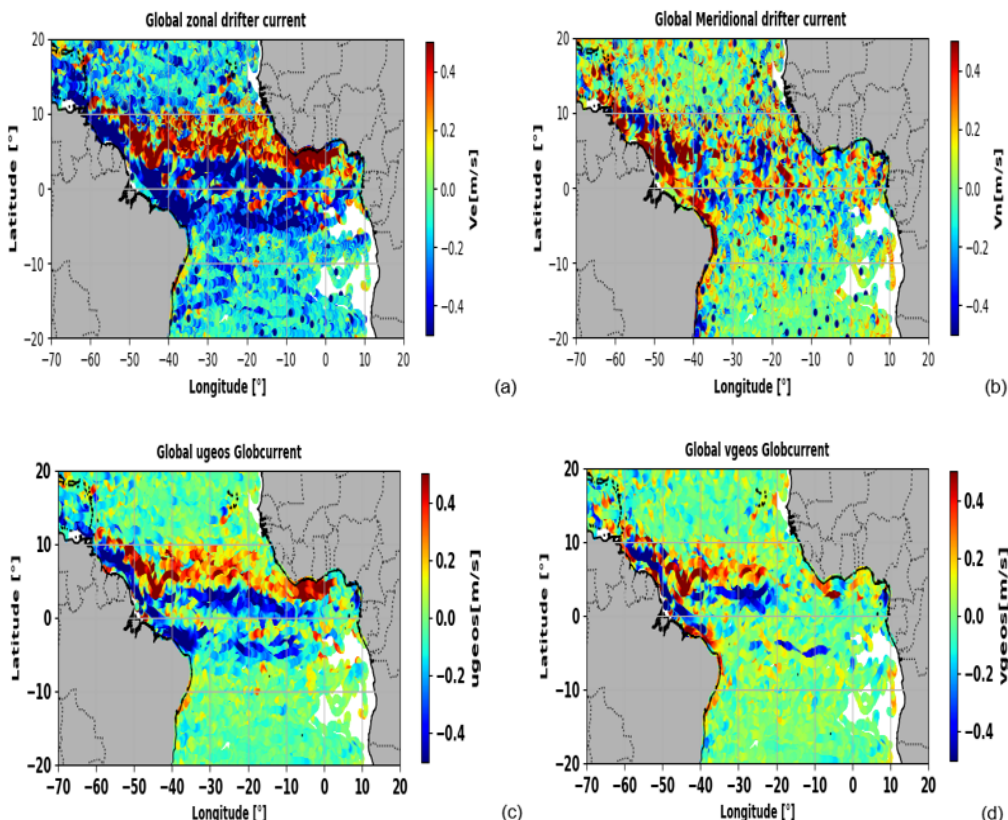


Figure 4.6 – Zonal and meridional currents of drifters (a, b), interpolated geostrophic currents from Aviso (c, d).

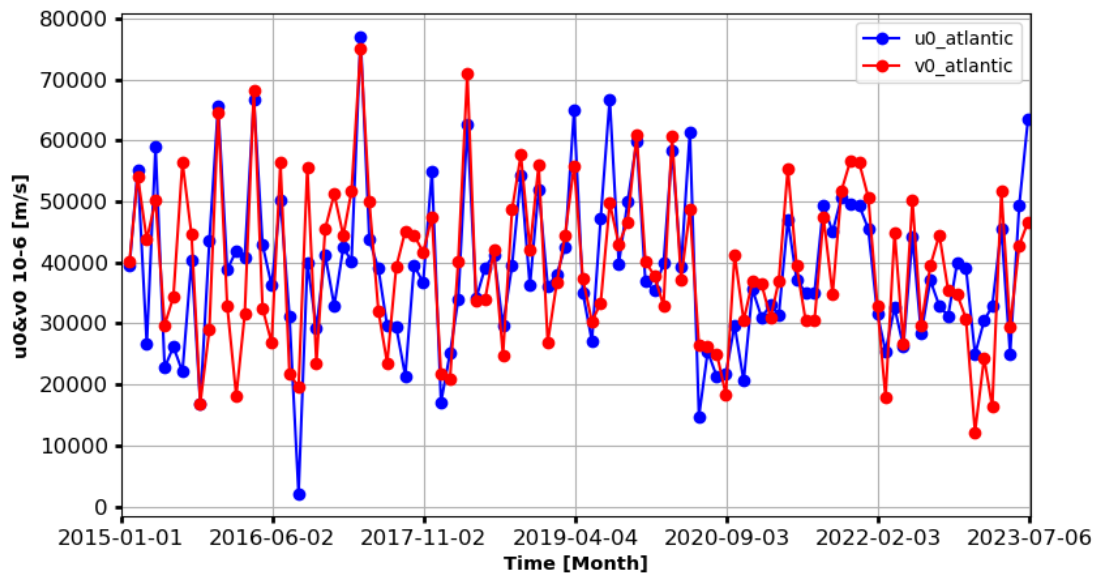


Figure 4.7 – Initial inertial speed: zonal u_0 in (blue) and meridional v_0 in (red).

Table 4.3 – Table comparing surface speeds from Glocurrent to the speeds of all drifters at 15 m in the region 20°N-20°S and 70°W-20°E.

Variables	Corr. Coef.	P-value	Regression Coef.	RMSE
(ugeos, u-drifter)	0.69	0.00	0.47	0.17
(vgeos, v-drifter)	0.44	0.00	0.31	0.17
(ugeos+ue, u-drifter)	0.77	0.00	0.60	0.15
(vgeos+ve, v-drifter)	0.50	0.00	0.36	0.15
(ugeos+ue, Hanning filter u-filtered)	0.83	0.00	0.72	0.12
Clemem filter	0.71	0.00	1.08	0.13
Median filter	0.78	0.00	0.61	0.14
(vgeos+ve, Hanning filter v-filtered)	0.60	0.00	0.53	0.12
Clemem filter	0.45	0.00	0.58	0.11
Median filter	0.51	0.00	0.37	0.15

Figure 4.7 shows that the initial components of the inertial speeds average 0.04 m/s, with maximum values around 0.08 m/s, due to the influence of continents on water circulation. Table 4.3 reveals that the Hanning filter most significantly improves the quality of surface currents from the drifters, with gains of 14% for the zonal component and 16% for the meridional component. The Ubelmann linear filter and the nonlinear median filter also show improvements but are slightly less effective than the Hanning filter.

Contribution of the SWOT Satellite to the Study

This chapter describes the design and objectives of the SWOT satellite and evaluates its impact on ocean surface currents by comparing its data with that from other satellites and in-situ measurements. The SWOT data used comes from 99 days of daily repeat in Fast Sampling mode. The satellite data includes sea surface height and geostrophic currents derived from the Globcurrent product of AVISO, available through the Copernicus Marine Service (CMEMS), while the in-situ comparisons are based on currents provided by NOAA's Global Drifter program.

5.1 Design and Objectives of the SWOT Satellite

The SWOT (Surface Water Ocean Topography) satellite, launched in 2022, is the result of a collaboration between CNES and NASA, with contributions from the UK and Canadian space agencies ([Fu et al., 2009](#); [Durand et al., 2010](#); [Morrow et al., 2019](#)).

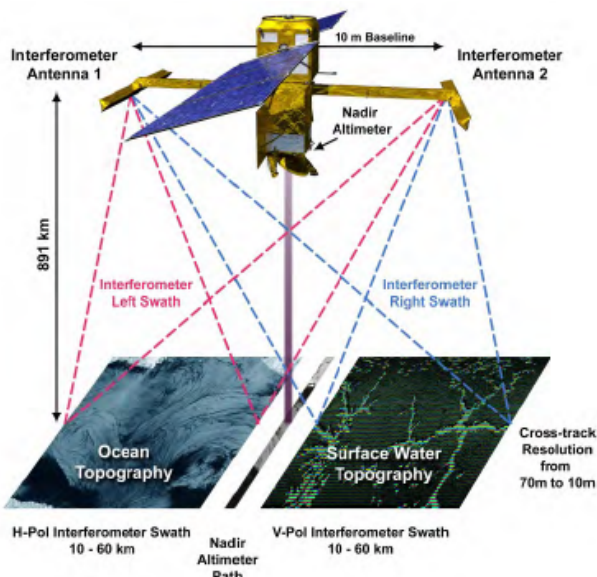


Figure 5.1 – Measurement principle of the SWOT satellite. Credits: NASA-JPL

Equipped with a Ka-band interferometric radar (KaRIn) (Durand et al., 2010; Fu and Ubelmann, 2014), as shown in Figure 5.1, it measures sea surface height (SSH) in two dimensions with unprecedented spatial resolution of 2 km. This radar offers an effective resolution of approximately 15-30 km, thanks to its 2D measurement and lower instrumental noise compared to conventional nadir altimeters (Dufau et al., 2016; Wang et al., 2019). The satellite captures data over two swaths of 50 km with a gap of 20 km around the nadir track. Its repeat cycle is 21 days, with a revisit time ranging from about 10 days at the equator to a few days at the poles. SWOT aims to enhance the global coverage of ocean mesoscale and sub-mesoscale variability (Wang et al., 2019).

5.2 Assessment Diagnostics

The comparison between the SWOT data, the Globcurrent product from AVISO, and the in-situ measurements from NOAA's Global Drifter program uses Pearson's correlation test, the slope coefficient, and the Root Mean Square Error (RMSE). This is done in two steps: first, the geostrophic currents from AVISO are compared to those estimated via SWOT, then the geostrophic currents from SWOT, to which an Ekman component has been added, are compared to those from the Global Drifter, after filtering out inertial oscillations. To perform these comparisons, it is necessary to place all data on a common grid, for example, that of SWOT. Then, we spatially interpolate the SWOT and AVISO data to the positions of the drifters.

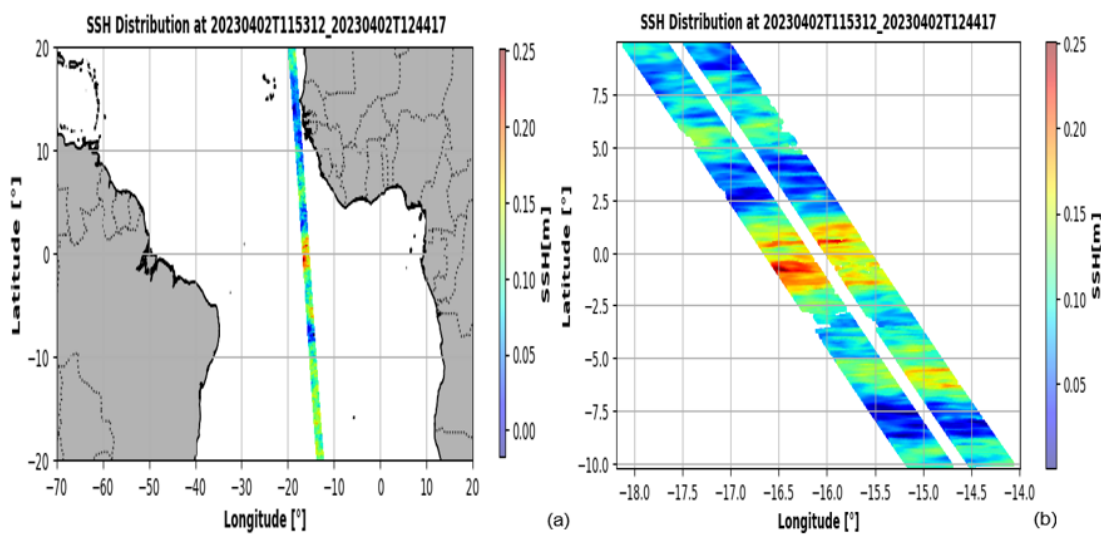


Figure 5.2 – Projection of SWOT sea surface height (SSH) in the tropical Atlantic (a) and an overview of its track (b).

5.2.1 Comparison of AVISO Geostrophic Currents with Those from SWOT

The interpolations of the geostrophic currents from AVISO and SWOT are illustrated in Figure 5.3. SWOT reveals a strong influence of small-scale variations, unlike AVISO. A spatial smoothing of $1/2^\circ$ shows that the green curves in Figure 5.4, representing the currents after filtering out small-scale variations, relatively reproduce the results from CMEMS, indicating good agreement at large scales. However, SWOT provides additional information at small scales, and it is crucial to verify the reality of these fine details by comparing them with data from drifting buoys. At large scales, SWOT and CMEMS are consistent, with a maximum correlation around 1° and acceptable from $1/2^\circ$, but degrading below that. This suggests that the high frequency in SWOT predominates over the low frequency signal, while the large-scale spatial variability of CMEMS becomes more visible after filtering. The comparison with drifting buoys will help confirm the accuracy of SWOT's fine details and its improvement over CMEMS.

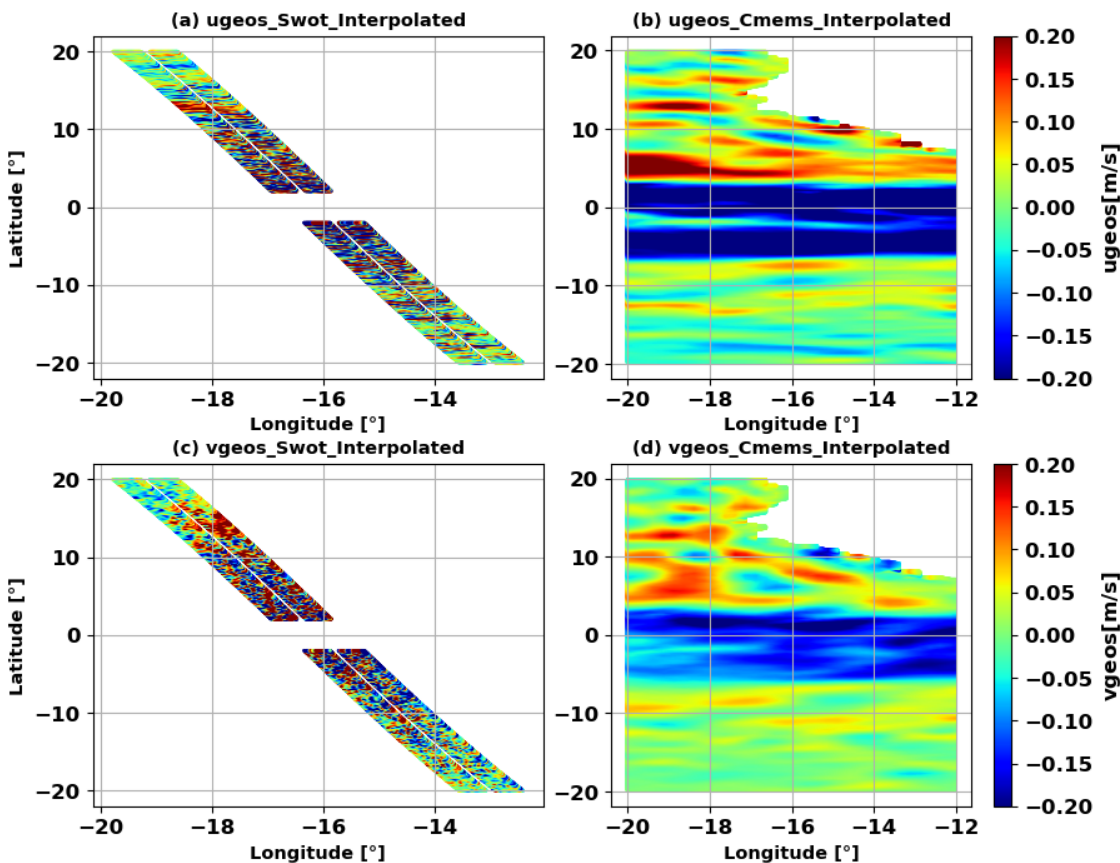


Figure 5.3 – Interpolation of SWOT and AVISO geostrophic currents on the SWOT grid: Zonal case (a, b) and meridional case (c, d).

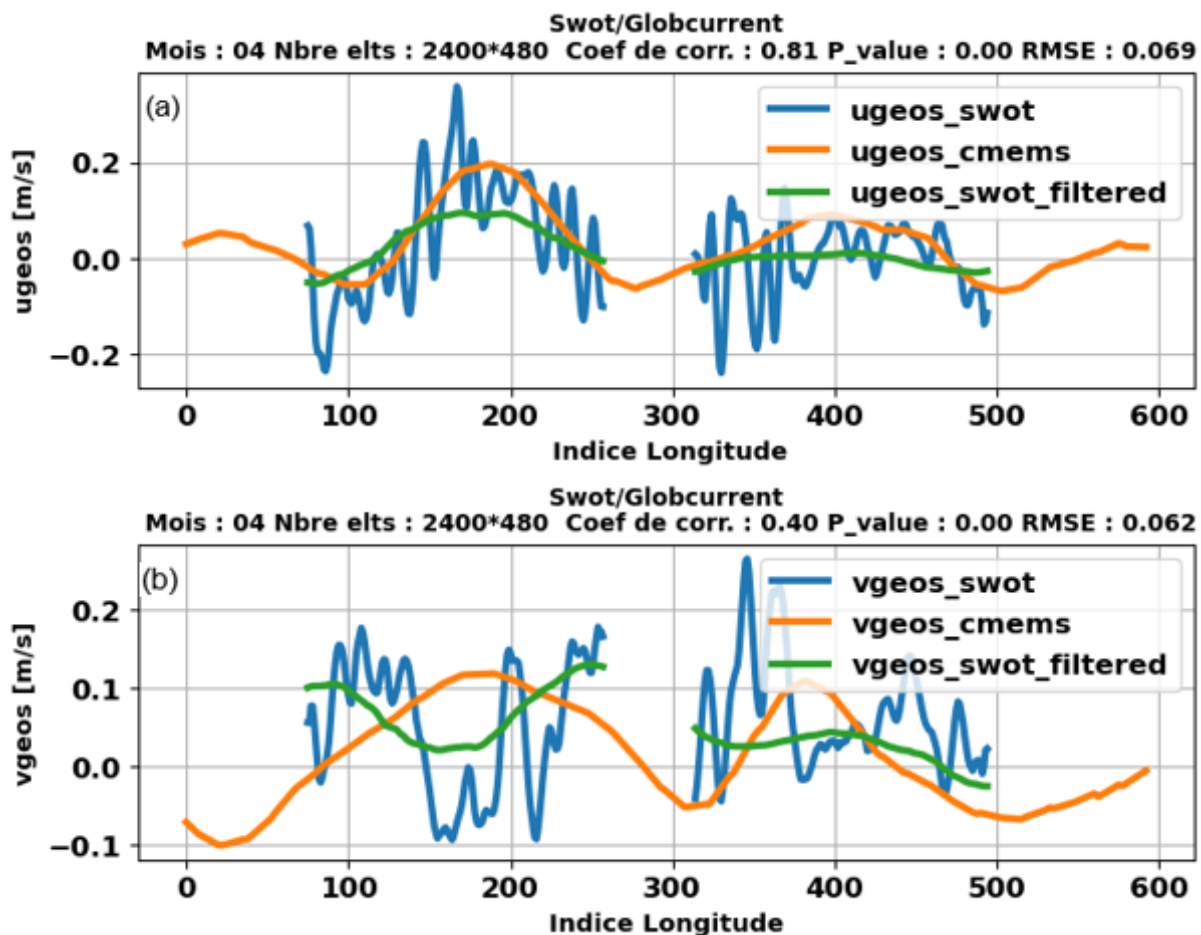


Figure 5.4 – Statistical analysis of spatial correlations between the interpolated geostrophic currents from SWOT and AVISO: Zonal case (a) and meridional case (b).

5.2.2 Comparison of SWOT Geostrophic Currents and Global Drifter

To compare the two sources of current data, we start by visualizing the trajectories of the drifters and the paths of the SWOT satellite. Figure 5.5 shows that the current measurements made by SWOT and AVISO coincide in certain areas, raising questions about the quality of surface ocean current measurements between the two products. For our analysis, we used a drifter covering the entire study period, alongside data from the SWOT and AVISO satellites. Figure 5.6 illustrates the overlay of the drifter's trajectory on the current fields of SWOT and AVISO.

The time series in Figures 5.7 and 5.8 indicate that the small-scale information in SWOT may not necessarily be realistic. However, after a temporal filtering

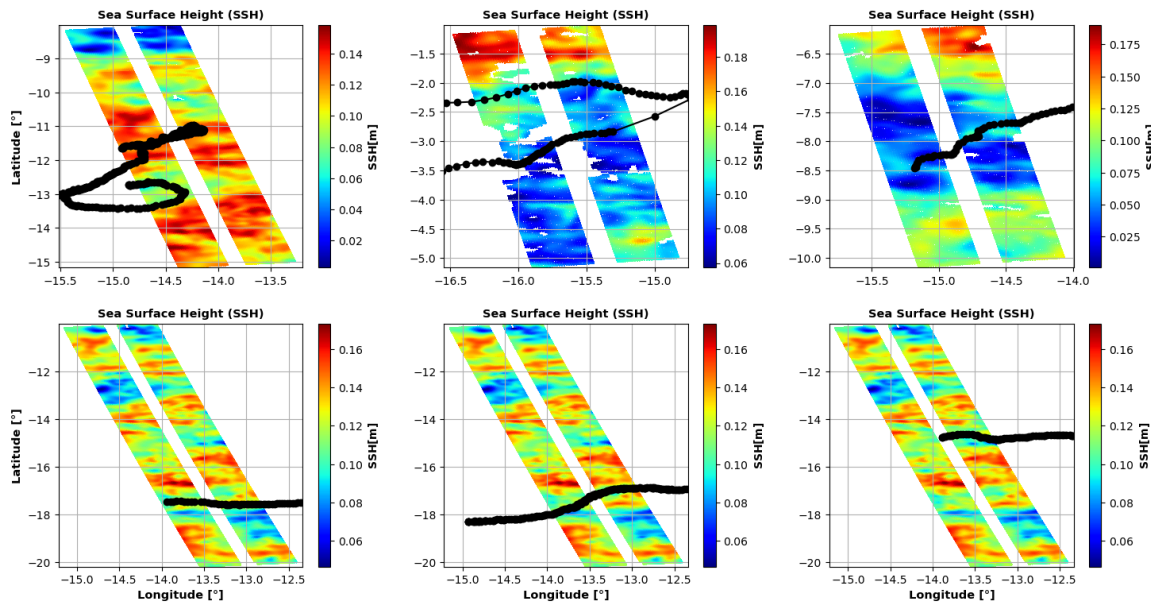


Figure 5.5 – SWOT trace for April 2, 2023, and the trajectory of the drifters.

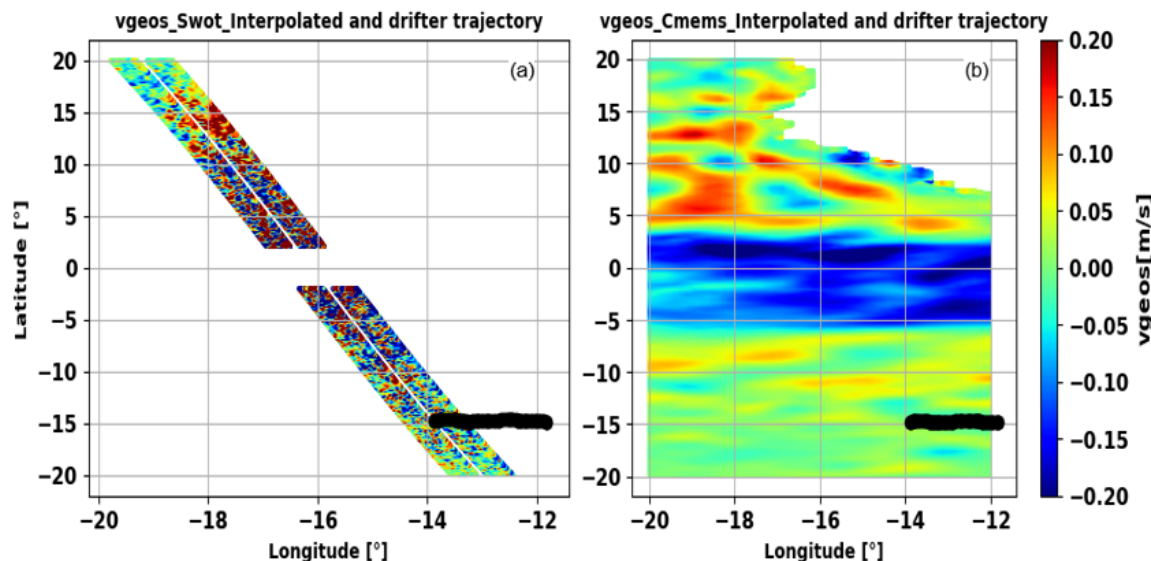


Figure 5.6 – Trajectory of the drifters superimposed on the meridional velocity fields of SWOT and CMEMS.

for 5 days, as indicated by the standard red curve in Figure 5.8, SWOT provides better information at the meso-scale compared to CMEMS, especially for the zonal component, where the resolution is adequate. In contrast, the meridional component is less precise due to insufficient coverage. Indeed, this component is derived from the sea surface height (SSH) measured along the longitude, and since the measurement band of the SWOT satellite is narrow but long, smoothing is performed over a large area according to latitude, which reduces the precision of this component.

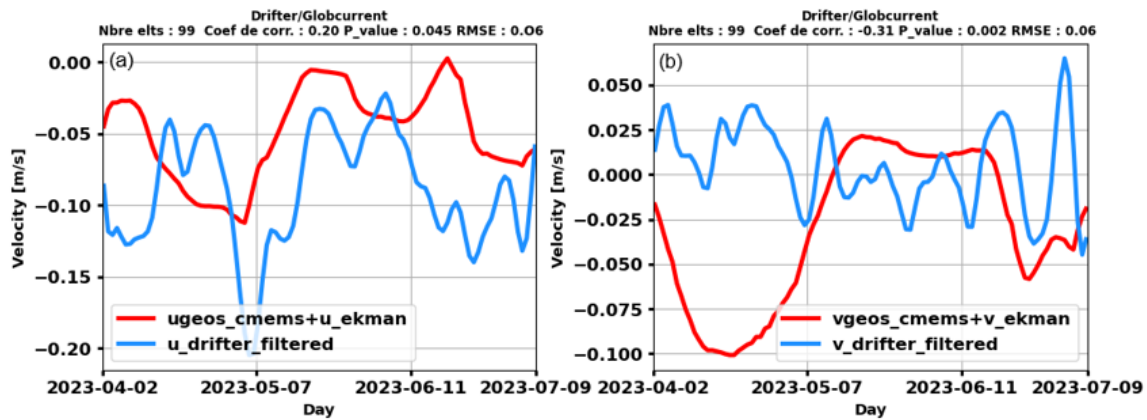


Figure 5.7 – Time series analysis between geostrophic currents from CMEMS and Drifter currents: Zonal case (a) and Meridional case (b).

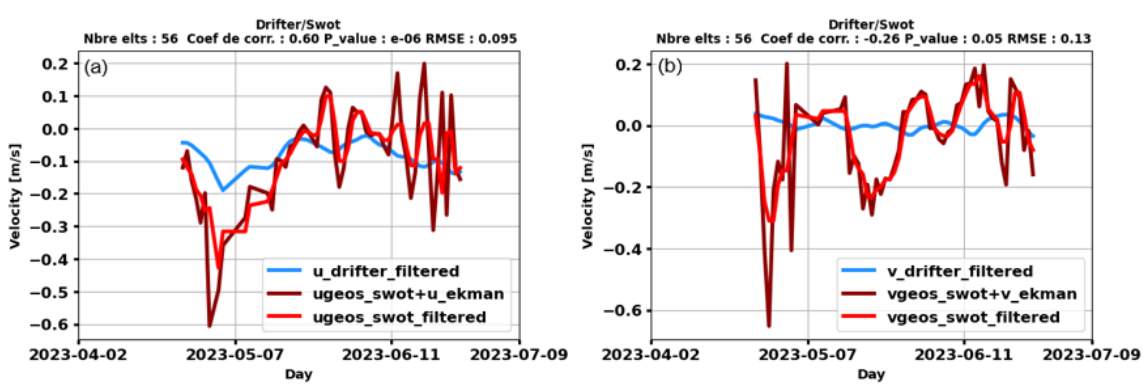


Figure 5.8 – Time series analysis between SWOT geostrophic currents and Drifter currents: Zonal case (a) and Meridional case (b).

5.3 Conclusion

In conclusion, the comparative analysis of geostrophic currents obtained from SWOT and AVISO, validated by in-situ measurements from the Global Drifter, reveals several key points. The initial comparison of geostrophic currents shows that SWOT and CMEMS are consistent on a large scale, although SWOT better captures small-scale variations. Statistical tests indicate that the small scales observed in SWOT may not be entirely realistic. However, after temporal filtering, SWOT provides improved information at the meso-scale compared to CMEMS, particularly for the zonal component. In contrast, the accuracy of the meridional component is reduced due to insufficient coverage of the swath width.

Conclusion and Recommendations

This study on the geostrophic and ageostrophic components of ocean currents, conducted through the combined analysis of data from drifting buoys and satellite products, has provided significant insights into the dynamics of surface currents. By utilizing data from the NOAA's Global Drifter Program and satellite products such as AVISO's Globecurrent and NRT SWOT KaRIn & nadir, we have highlighted the advantages and limitations of these various data sources. The results show that AVISO altimetry provides a low-resolution Eulerian description of geostrophic currents. SWOT data are consistent with AVISO at low resolution and provide information at a smaller scale. We assessed the contribution of this small scale by comparing SWOT data with drifter data. This required considering various ageostrophic components (filtering of inertial oscillations for the drifters and adding an Ekman component to the geostrophic velocities derived from SWOT). After spatial and temporal filtering, SWOT data showed significant improvement for the zonal component but limited improvement for the meridional component. This was interpreted as being related to the specific characteristics of the SWOT track.

A significant part of this work was based on the development of programs for spatial and temporal filtering of the data. It was particularly shown that inertial oscillations have a significant signature on drifter currents, and it is necessary to filter them. The linear Hanning filter proved to be particularly effective in improving the quality of surface currents from drifters, with significant improvements in estimating the zonal and meridional geostrophic components.

These results highlight the need to refine marine data filtering methods to reduce the errors of current techniques, optimize SWOT data by widening the swath to better measure the meridional component, and further exploit drifter data to validate the velocity components from SWOT.

Bibliography

- [1] Assassi, C., Morel, Y., Vandermeirsch, F., Chaigneau, A., Pegliasco, C., Morrow, R., Colas, F., Fleury, S., Carton, X., Klein, P., & Cambra, R. An index to distinguish surface- and subsurface-intensified vortices from surface observations. *Journal of Physical Oceanography*, 46(8), 2529–2552. <https://doi.org/10.1175/JPO-D-15-0122.1> (2016).
- [2] Bourles, B. Cours d'introduction à l'océanographie physique, MASTER2 « Océanographie Physique et Applications», version 2 (novembre 2008), Chap. 4, pp. 50-64, Chap. 5, pp. 90-96, pp. 100-109. (2008).
- [3] Brock, F. V., A nonlinear filter to remove impulse noise from meteorologicadla ta,J . Atmos. OceanicT echnol.3, , 52-58, (1986).
- [4] Chelton, D. B., M. G. Schlax, and R. M. Samelson. Global obser-vations of nonlinear mesoscale eddies. *Prog. Oceanogr.* 91: 167–216. <https://doi.org/10.1016/j.pocean.2011.01.002> (2011).
- [5] Chaigneau, A., Gisolme, A., & Grados, C. Mesoscale eddies off Peru in altimeter records: Identification algorithms and eddy spatio-temporal patterns. *Progress in Oceanography*, 79, 106–119. <https://doi.org/10.1016/j.pocean.2008.10.013> (2008).
- [6] Daniault, N. Cours Océnographie physique, Ecole Navale, Université de Bretagne Occidentale, p. 79, p.6. (2005).
- [7] Dohan, K., and N. Maximenko. Monitoring ocean currents with satellite sensors. *Oceanography* 23: 94–103. <https://doi.org/10.5670/oceanog.2010.08> (2010).
- [8] Dufau, C., Orsztynowicz, M., Dibarboire, G., Morrow, R., and Traon, P.-Y. L. Mesoscale resolution capability of altimetry: Present and future. *J. Geophys. Res. Oceans*, 121, 4910–4927. <https://doi.org/10.1002/2015JC010904> (2016).
- [9] Durand, M., Fu, L., Lettenmaier, D. P., Alsdorf, D. E., Rodriguez, E., and Esteban-Fernandez, D. The Surface Water and Ocean Topography Mission: Observing Ter-restrial Surface Water and Oceanic Submesoscale Eddies. *Proc. IEEE*, 98, 766–779. <https://doi.org/10.1109/JPROC.2010.2043031> (2010).
- [10] Durran, D. R. Is the Coriolis force really responsible for the inertial oscillation?. *Bulletin of the American Meteorological Society*, 74(11), 2179-2184. (1993).

- [11] Fu, L.-L., Alsdorf, D., Rodriguez, E., Morrow, R., Mognard, N., Lambin, J., Vaze, P., and Lafon, T. The SWOT (Surface Water and Ocean Topography) Mission: Spaceborne Radar Interferometry for Oceanographic and Hydrological Applications. (2009a).
- [12] Fu, L.-L., Alsdorf, D., Rodriguez, E., Morrow, R., Mognard, N., Lambin, J., Vaze, P., and Lafon, T. The SWOT (Surface Water and Ocean Topography) Mission: Spaceborne Radar Interferometry for Oceanographic and Hydrological Applications. (2009b).
- [13] Holton, J. R. Introduction to Dynamic Meteorology, 3rd Ed. Academic Press, 511 pp. (1992).
- [14] Hermozo, L. L'estimation de la correction troposphérique humide pour l'altimétrie spatiale: l'approche variationnelle. Diss. Université Paul Sabatier-Toulouse III. (2018).
- [15] Lagerloef, G. S. E., et al. Tropical Pacific near-surface currents estimated from altimeter, wind, and drifter data. *Journal of Geophysical Research: Oceans*, 104(C10), 23313-23326. (1999).
- [16] Liu, H., et al. Opposite-Sign Sea Surface Salinity Anomalies Over the Northeastern and Southwestern South Atlantic Ocean From 2010 to 2017. *Journal of Geophysical Research: Oceans*, 127(12), e2022JC019351. (2022).
- [17] Lumpkin, R., and M. Pazos. Measuring surface currents with Surface Velocity Program drifters: The instrument, its data and some recent results. Pp. 39–67. In A. Griffa, A. D. Kirwan, A. J. Mariano, T. Ozgokmen, and T. Rossby [eds.], *Lagrangian Analysis and Prediction of Coastal and Ocean Dynamics (LAPCOD)*. Cambridge University Press. <https://doi.org/10.1017/CBO9780511535901.003> (2007).
- [18] Morrow, R., Fu, L.-L., Ardhuin, F., Benkiran, M., Chapron, B., Cosme, E., d'Ovidio, F., Farrar, J. T., Gille, S. T., Lapeyre, G., Le Traon, P.-Y., Paschal, A., Ponte, A., Qiu, B., Raschle, N., Ubelmann, C., Wang, J., and Zaron, E. D. Global Observations of Fine-Scale Ocean Surface Topography With the Surface Water and Ocean Topography (SWOT) Mission. *Front. Mar. Sci.*, 6. <https://doi.org/10.3389/fmars.2019.00232> (2019a).
- [19] Morrow, R., Fu, L.-L., Ardhuin, F., Benkiran, M., Chapron, B., Cosme, E., d'Ovidio, F., Farrar, J. T., Gille, S. T., Lapeyre, G., Le Traon, P.-Y., Paschal, A., Ponte, A., Qiu, B., Raschle, N., Ubelmann, C., Wang, J., and Zaron, E. D. Global Observations of Fine-Scale Ocean Surface Topography With the Surface Water and Ocean Topography (SWOT) Mission. *Front. Mar. Sci.*, 6. <https://doi.org/10.3389/fmars.2019.00232> (2019b).

- E. D. Global Observations of Fine-Scale Ocean Surface Topography With the Surface Water and Ocean Topography (SWOT) Mission. *Front. Mar. Sci.*, 6. <https://doi.org/10.3389/fmars.2019.00232> (2019b).
- [20] Niiler, P. P., N. A. Maximenko, and J. C. McWilliams. Dynamically balanced absolute sea level of the global ocean derived from near-surface velocity observations. *Geophys. Res. Lett.* 30: 2164–2168. <https://doi.org/10.1029/2003GL018628> (2003).
- [21] Pegliasco, C. Structure verticale des tourbillons de mésoscalaire dans les quatre grands systèmes d'upwelling de bord est [Université Paul Sabatier - Toulouse III]. <https://tel.archives-ouvertes.fr/tel-01427163> (2015).
- [22] Picaut, J., and R. Tournier. Monitoring the 1979–1985 equatorial Pacific current transports with expendable bathythermograph data. *J. Geophys. Res.* 96 (Suppl.): 3263–3277. (1991).
- [23] Picaut, J., Busalacchi, A. J., McPhaden, M. J., & Camusat, B. Validation of the geostrophic method for estimating zonal currents at the equator from Geosat altimeter data. *Journal of Geophysical Research: Oceans*, 95(C3), 3015-3024. (1990).
- [24] Persson, A. The Coriolis effect—a conflict between common sense and mathematics. Italian Meteorological Society, 20-31. (2005).
- [25] Ralph, E. A., and Pearn P. Niiler. Wind-driven currents in the tropical Pacific. *Journal of Physical Oceanography*, 29(9), 2121-2129. (1999).
- [26] Richardson, P. L. Worldwide ship drift distributions identify missing data. *J. Geophys* (1989).